PERGAMON

Continental Shelf Research 21 (2001) 667–695

CONTINENTAL SHELF RESEARCH

www.elsevier.com/locate/csr

Seasonal mean circulation in the Yellow Sea — a model-generated climatology

Christopher E. Naimie[a], Cheryl Ann Blain[b], Daniel R. Lynch[a,*]

[a] *Dartmouth College, Hanover, NH, 03755, USA*

[b] *Naval Research Laboratory, Ocean Dynamics and Prediction Branch, Stennis Space Center, MS, 39529-5004, USA*

Received 4 May 1999; accepted 8 March 2000

Abstract

The three-dimensional climatological circulation is computed for the Yellow and Bohai Seas in a series of six bimonthly realizations. The model (QUODDY, Lynch et al., Continental Shelf Res. 16(7) (1996) 875) is nonlinear, tide-resolving, and baroclinic with level 2.5 turbulence closure. Data inputs include seasonal hydrography, seasonal mean wind and river input, and oceanic tides. Results for winter and summer exhibit two distinct circulation modes. In winter, strong northerly wind drives southward flow at the surface and along both Korean and Chinese coasts. This is compensated by deep return flow — the Yellow Sea Warm Current — in the central trough of the Yellow Sea, penetrating to the Bohai. The Changjiang discharge exits to the southwest in winter, trapped along the Chinese coast. In summer, a water mass produced by winter cooling — the Yellow Sea Cold Water — is isolated in the deep central trough, setting up cyclonic circulation over the eastern Yellow Sea. Summer winds from the south drive northeastward flow along the Chinese coast. The net result is a qualitative reversal of the winter pattern. The Changjiang discharge is driven offshore toward the Korean Strait by the summer wind. The winter and summer circulations are partitioned dynamically among tidal rectification, baroclinic pressure gradients, wind response, and river input from the Changjiang. Wind dominates the winter pattern. In summer, baroclinic pressure gradients dominate the eastern Yellow Sea; with wind, tidal rectification, and input from the Changjiang dominant to the west of the cyclonic gyre. The seasonal cycle indicates that January and March exhibit the same basic winter pattern. May is quiescent, followed by July which defines the summer mode. September shows the same general summer pattern, with features shifted westward. November is a transition period followed by winter conditions.

Keywords: Seasonal cycle; Climatology; Yellow Sea

*Corresponding author. Fax: +1-603-646-3856.

E-mail address: d.r.lynch@dartmouth.edu (D.R. Lynch).

0278-4343/01/$ - see front matter
PII: S0278-4343(00)00102-3

1. Introduction and overview

The Yellow Sea (YS) is a shallow, relatively flat shelf sea enclosed on three sides by China and the Korean peninsula (Fig. 1.) Its long axis extends inland from the East China Sea (ECS) approximately 1000 km, with depth less than 100 m. The major bathymetric feature is a central trough along this axis, penetrating to the Bohai Sea (BS). Its seaward connection to the ECS occurs over a broad shelf, with shelf break at the 200 m isobath extending roughly along a line connecting Taiwan and Japan.

Three major ECS features influence the Yellow Sea. The Kuroshio at the shelf break, and the Taiwan Warm Current (TWC) on the ECS shelf, flow generally to the Northeast through the ECS and influence the Yellow Sea hydrography, circulation and dynamics. (See Fig. 2 from Su, 1998.)

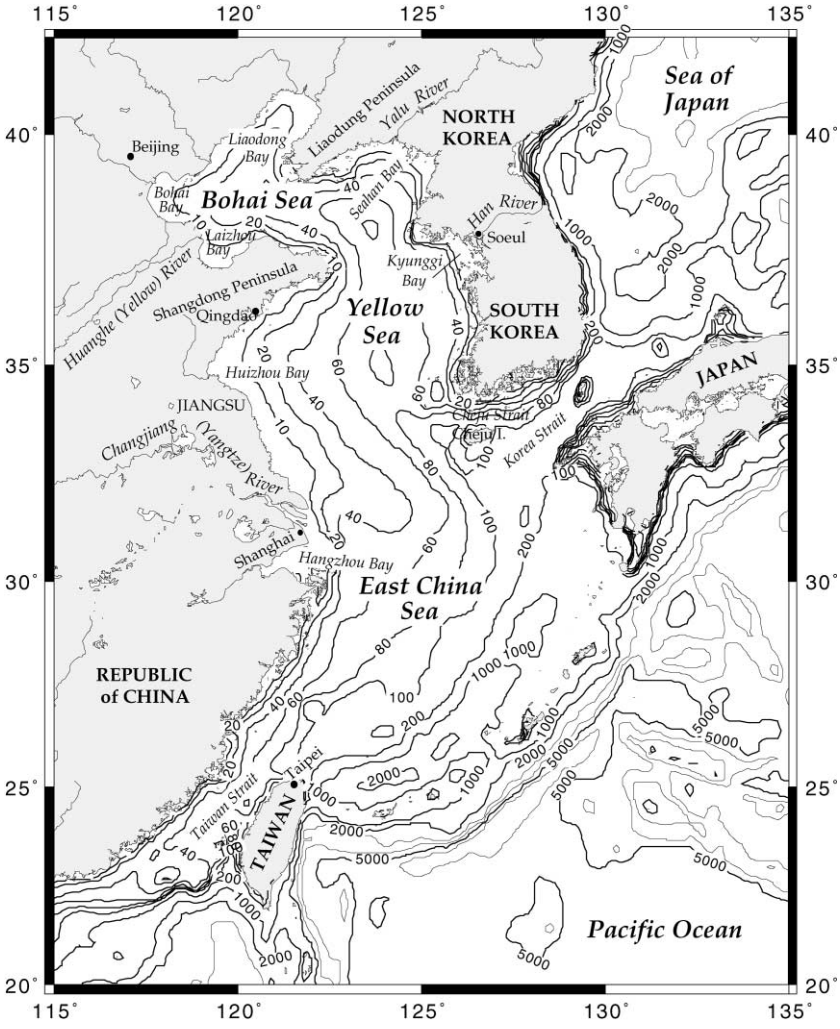

Fig. 1. Topography and geography.

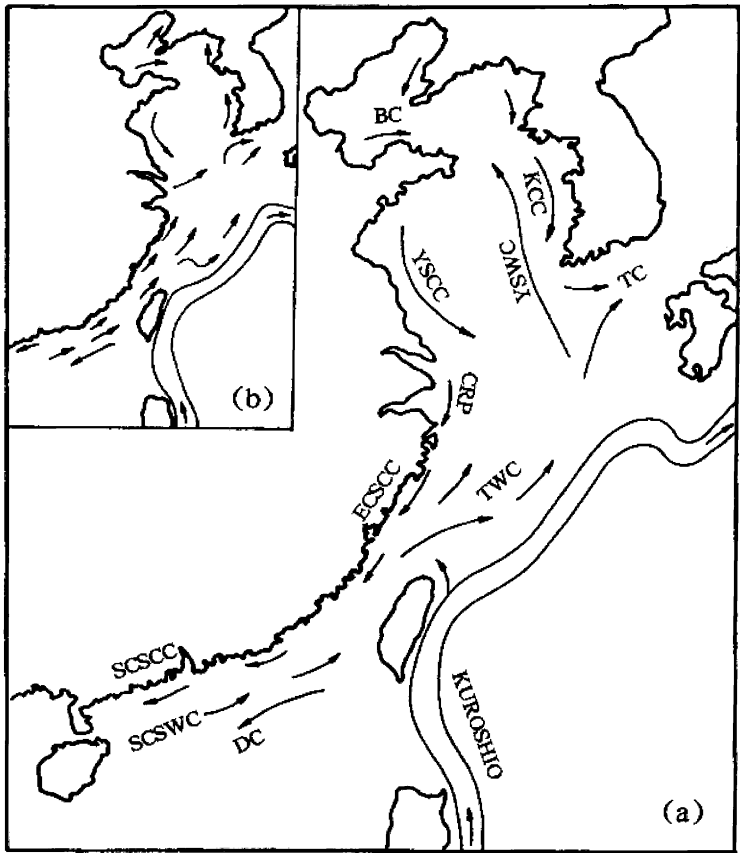

Fig. 2. (a) Winter and (b) summer circulation features for the China Seas, from Su (1998). The current features identified are the Bohai Coastal Current (BC), the Yellow Sea Coastal Current (YSCC), the Changjiang River Plume (CRP), the East China Sea Coastal Current (ECSCC), the Taiwan Warm Current (TWC), the Tsushima Current (TC), the Yellow Sea Warm Current (YSWC), the Korean Coastal Current (KCC), the South China Sea Coastal Current (SCSCC), the South China Sea Warm Current (SCSWC), and the Dongsha Current (DC).

Additionally, the Changjiang (formerly Yangtze) River (world's fourth largest) discharges at the junction of the Yellow and East China Seas. Recent oceanographic overviews are provided by Seung and Park (1989) and Su (1998). Also, the edited volume Zhou et al. (1994), contains overviews of hydrography (Su and Weng, 1994), circulation (Guan, 1994; Hu, 1994) and tides (Fang, 1994).

Atmospheric Interaction. Strong northerly winds generally prevail over the Yellow Sea during winter months, while the summer is characterized by weak southerly winds. During winter, wind-generated turbulence enhances deep cooling by thermal convection. During summer, the weaker and less persistent winds combine with surface heating to result in very strong thermal stratification, isolating the bottom water (see below).

Hydrography. The hydrographic structure reveals two distinct features. The Yellow Sea Warm Current (YSWC) — a tongue of warm salty water of TWC/Kuroshio origin — is observed extending northward as far as the Bohai Sea during winter. Historically described as a branch of

the Kuroshio and/or the TWC, it is currently thought to originate as return flow compensating the wind-driven southward flow in winter. The Yellow Sea Cold Water (YSCW) — a water mass regarded as a remnant of winter cooling and mixing — is observed in the deeper locations during summer. Discussion of these features dates back to the work of Uda (1934).

Freshwater Runoff. The most significant freshwater discharge in the region is from the Changjiang, with annual mean inflow of $28,900\ m^3\ s^{-1}$ (Riedlinger and Preller, 1995). During winter, the Changjiang discharge is thought to exit southwestward along the Chinese coast. During summer, a more intense and variable discharge spreads offshore to the northeast, generally following the pathway of the TWC. The second largest river in the region is the Huanghe. It discharges into the Bohai Sea, with an annual flow of approximately 1/20th of that for the Changjiang. Annual mean and seasonal input values for the major rivers in the region, are reported in Riedlinger and Preller (1995).

Tides. The tides are mixed diurnal/semidiurnal, with M2 and K1 amplitudes of order 1.0 and 0.25 m, respectively. The semidiurnals in particular have complex spatial structure. In some regions, tidal currents are sufficient to create permanent mixing fronts. In addition to their role in summer-time frontogenesis, rectification of large tidal currents nearshore is likely to contribute to subtidal circulation patterns year-round.

Circulation. General circulation patterns are summarized in the map of Su (1998), (Fig. 2). There are two distinct modes. In winter, the strong northwesterly winds drive surface and nearshore transport southward, demanding a northward return flow at depth. This flow originates as warm, salty TWC water, and explains the observed YSWC. Nearshore coastal currents are southward (downwind) on both Korean and Chinese coasts under this wind-dominated scenario. During summer, the dense YSCW dominates the central Yellow Sea, resulting in a basin-scale low-pressure system and cyclonic circulation. Wind forcing during this period is significantly reduced and in the opposite direction relative to the winter, resulting in an interruption of the northward flow associated with the TWC. Under this scenario, coastal currents would be directed northward along Korea and southward along China. Local enhancements may be expected year-round due to tidal rectification; and in summer, due to freshwater inputs and tidal mixing fronts.

Our Goal is to describe the 3-D climatological mean circulation in the Yellow and Bohai Seas. We consider forcing from semi-diurnal and diurnal tidal constituents, baroclinic pressure gradients, wind, exchange with the ECS, and inflow from the Changjiang. We reproduce the two principal modes described above, partition the dynamics, and provide an approximation of the yearly cycle in six quasi-static "seasonal" snapshots. The general procedure follows that used by Naimie (1996) and Lynch et al. (1997) for Georges Bank and the Gulf of Maine. We initialize from a seasonal hydrographic database; compute prognostically to allow short-term tidal-time adjustment; and then capture and analyze the quasi-steady subtidal fields.

2. Circulation modeling review

There are over 20 years of accumulated modeling experience in the Yellow Sea. The majority of studies deal primarily with tides, and there are notable early successes. Subtidal circulation modeling has received less attention, but with steadily increasing sophistication. Several studies in

this category are focused primarily on ECS features and dynamics i.e. offshore from our principal interest.

2.1. Tidal dynamics

An (1977) constructed the first modern tidal model of the Yellow and Bohai Seas. He used a 2-D finite difference model in cartesian coordinates, with seaward boundary running from Shanghai to Korea, and horizontal resolution of 11 km. This study focused on the M2 constituent, for which good qualitative agreement with historical data (Ogura, 1941) was reported. The tide generating potential was included; however it was found that its effect was minor, contributing only 3% to the response.

Choi (1980) applied a similar nonlinear 2-D model with resolution $1/5 \times 1/4^\circ$ (approximately 22 km). The seaward boundary was placed further out in the ECS, at roughly the 200 m isobath. The tide generating potential was neglected. The study included the four constituents M2, S2, K1, and O1. Data were taken from Ogura (1933). Typical M2 elevation errors were 10% amplitude and 10° phase, at approximately 60% of the observational locations. The tidal residual velocity was examined, but it was suggested that the resolution was insufficient for this purpose. This is the baseline tidal modeling study in the region, having been used by several subsequent investigators. It displays a characteristic 4-amphidrome system for the semidiurnals, and a 2-amphidrome system for the diurnals. Choi (1984) extended this study to 3-D, with advection neglected, constant vertical viscosity, and M2 forcing only. Elevation results were similar to the previous 2-D result, except in the Gulfs of Bohai and Liaodung. Comparison with nine current measurements offshore of the Changjiang showed agreement to within roughly 10–15 cm/s and 10° phase. This velocity comparison was extended by Larsen et al. (1985). In addition, Larsen et al. (1985) review historical elevation observations (Ogura, 1933) and the Choi calculations. They attributed disagreement in Liaodung Gulf to poor grid resolution; and along the Chinese coast to uncertainty and/or time-variations in bathymetry. Choi (1990) tripled the resolution to $1/15 \times 1/12^\circ$ in a 3-D M2 model. The focus was on current meters (six moorings with 1 or 2 vertical positions each) along the central Yellow Sea trough and near South Korea. Agreement was roughly 15–20% amplitude, 10–15° phase.

Lie (1989) studied tidal mixing fronts, using a Choi-like model (2-D, barotropic, $1/5 \times 1/4^\circ$; same general geographic coverage) to compute the M2 and the Simpson and Hunter (1974) mixing parameter. Three mixing regions along Korea are identified (southwest tip; southern Kyunggi Bay; and Seohan Bay). Another mixing region was identified along the mid-east coast of China. The Korean coast fronts were verified from observed SST images.

Kang et al. (1991) computed the M2 tide over the Yellow, East China, and Japan Seas with a 2-D, $1/8 \times 1/6^\circ$ model. Data from Nishida (1980) are introduced to update/replace the Ogura standard. The four amphidrome M2 system from the Choi studies was reproduced. The tide-generating force was included and it was found to contribute several percent to the tidal amplitude. The effect is much stronger in the Japan Sea. This is generally consistent with An (1977). In a subsequent study, Kang et al. (1998) doubled the resolution to $1/16 \times 1/12^\circ$, and broadened the spectrum to include M2, N2, S2, O1, K1 plus M4 and MS4. The domain excluded the Sea of Japan, but extended seaward of the Choi domain. The RMS differences between modeled and observed M2 tidal elevations were 9.7 cm/4.5°. For the tidal current observations in

the central Yellow Sea, they reported M2 tidal current errors of order of 3–4 cm/s speed, 10–20° phase, and significantly larger errors at other stations. The tide generating force modified the M2 and S2 responses by about 5%; the effect is less for the other constituents.

Yanagi and Inoue (1994) computed a 2-D solution on a β-plane at 25 km resolution, which is a comparable resolution to that of Choi (1980). By comparison with Choi's results, it was concluded that both β-plane and f-plane approximations yielded equivalent results (tides and residual) to spherical-polar calculations.

Blain (1996) applied a 2-D nonlinear model (Kantha, 1995) to the YS/BS/ECS region. Horizontal resolution was $1/5^\circ$ and tidal potential forcing was included. The model assimilated observed tidal elevations via nudging for a spectrum of eight constituents (M2, N2, S2, K2, O1, K1, P1, Q1). A new 114-station composite data base was used, taken from International Hydrographic Office data (IHO, 1979) and altimetry (Desai and Wahr, 1994). The data assimilation strategy reduced model errors by as much as a factor of 2, with the resulting M2 and K1 amplitude errors being approximately 13% of measured values. Blain (1997) extended this study to include M4 and MS4. Assimilation of partial data sets revealed that (a) deep (over 200 m) data had little effect on model skill; (b) shallow (between 10 and 200 m deep) data were most important; (c) coastal data (under 10 m deep) added skill for the nonlinear constituents; and (d) the number of data points was less important than their broad distribution.

Kantha et al. (1996) reported results with the same data-assimilative model. This study included the Sea of Japan, at comparable resolution. Forcing was limited to the M2 and S2 constituents; with a focus on the generation of residual and overtides (M4, S4, MS4, M6, ...). General agreement with earlier studies (Kang, Choi) was found for the M2 and S2. Large M4 phase errors were attributed to poor resolution and/or lack of data to assimilate. Residual velocity maps were shown for M2 and S2 separately. As in previous studies, residual speeds were small, of order 2 cm/s.

Several tidal studies have been reported for the Bohai Sea, where the larger regional models have had difficulty matching tidal elevation observations. Xie et al. (1990) applied a 2-D model to the Bohai. Resolution was 3 km and forcing included the M2, S2, N2, K1, and O1 constituents. Changes in the amphidromic structure with respect to early studies (Ogura, 1933; Choi, 1980) were attributed to sedimentation. M2 elevation errors at 9 stations were of order 10 cm and 8°. Generally, a poor tidal match was found in the southwest Bohai. The tidal residual current was weak — 2 cm/s or less — with hot spots of order 10 cm/s. There is a large anticyclonic circulation in the center of the Bohai; a cyclonic gyre to its west in the Bohai Bay, and smaller structures in Laizhou and Liaodong Bays.

Sun et al. (1990) applied a coarser 3-D tidal model of the Bohai, with a horizontal resolution 14.4×18.5 km and 4 z-levels. They reported M2 elevation errors of order 5 cm and 5° at six locations. The tidal residual was qualitatively similar to that of Xie et al. (1990).

Huang (1991) calculated the M2, S2, K1 and O1 tides in the Bohai with a $1/12^\circ$ 2-D model. They considered bathymetry characteristic of the 1930s and the 1970s. A significant change was noted in the semidiurnals due to boundary and bathymetric changes over time. The diurnals showed only a slight change.

Dou et al. (1994) described a 3-D, barotropic, f-plane model of the M2, S2, K1, O1 tides in the Bohai. Horizontal resolution is approximately 10 km (roughly $1/10 \times 1/8^\circ$) and there with

10 σ-layers in the vertical. The M2 agreement was 7.4 cm, 16.7° RMS; K1, 6.3 cm, 25.9° at the nine coastal tidal stations considered.

Summarizing the tidal modeling work to date: the Choi (1980) 2-D result is a benchmark and widely cited. He established baseline accuracy (10% amplitude, 10°) at a subset of stations; and the baseline structure for semidiurnals (4 amphidromes) and diurnals (2 amphidromes). Both f- and β-planes generally work as well as spherical; and the tide-generating potential is not important unless deep water (e.g. Sea of Japan, ECS beyond the shelf break) is modeled. 2-D calculations are performing as well as 3-D for elevation comparisons. There is very limited tidal current data, but modeled tidal velocities produce realistic Simpson–Hunter mixing fronts. There has been limited attention to tidally rectified circulation except in the Bohai Sea. The Bohai itself has presented the most problems for modelers, partly due to topographic changes over time.

There may be a shifting data standard for both tide and topography. There has been widespread use of very early data (Ogura, 1933); later supplemented by Nishida (1980), and most recently with altimetry. Detailed comparison of the various sources with each other is unknown. The more recent model studies do not generally show higher accuracy.

2.2. Subtidal circulation

2.2.1. East China Sea

Several modeling studies have focused on the ECS features (TWC, Kuroshio, Changjiang) at the edge of the Yellow Sea. Yuan et al. (1986) diagnosed August 1981 hydrographic and velocity data in the Changjiang discharge area. The model was 3-D, steady, linear, diagnostic, with constant vertical viscosity. They found that the TWC passes through the study region and dominates the water column. It turns gradually toward the Northwest, following the topography.

Yuan et al. (1987) made a similar 3-D diagnosis for summer and winter, in the region between Taiwan and Shanghai. The TWC was the dominant feature in both seasons (i.e seasonal wind forcing did not play an important role). They discussed two branches of the TWC, Inshore and Offshore. In both seasons, the Offshore Branch originated in the Kurishio as it invaded the shelf. The Inshore Branch originated in Taiwan Strait in summer, while in winter it seemed to come from the Kuroshio with an ambiguous contribution from Taiwan Strait. In winter there is a strong coastal front. Inshore of the front the flow is to the SW. East of the front the subsurface TWC flows to the NW, against the wind. They conclude that the Tsushima Current originates from the TWC, not as a separate branch of the Kuroshio.

Chao (1991) studied the interplay of TWC, Kuroshio, Changjiang discharge, and wind forcing in the ECS. Included is an excellent review of observations, corroborating several points made by Yuan et al. (1987). A 3-D nonlinear primitive equations model was used. The domain is a highly idealized representation of the shelf/slope topography with horizontal resolution of 20 km and 10 vertical levels. They specified uniform vertical eddy viscosity and did not include tidal forcing. Their results indicate large barotropic contributions to TWC from both sides of Taiwan in the absence of wind. They also found that the winter wind weakens the Taiwan Strait contribution to the TWC; while the summer wind strengthens it. At the Changjiang plume, a near-field bimodal distribution in summer resulted from upwelling-favorable wind. In winter, downwelling-favorable wind confined the Changjiang discharge to a nearshore coastal jet flowing southward.

2.2.2. Yellow Sea

Yuan and Su (1984) presented a 2-D diagnostic model for steady winter (single layer) and summer (2-layer) circulation. Horizontal resolution was approximately $1/2^\circ$ in winter and 1° in summer. The winter results showed a 2-gyre structure with northward flow of the YSWC against the wind in the central trough and a coastally trapped Changjiang discharge. The summer results are very complex and underresolved; generally a reversal of the winter pattern was found.

Hsueh et al. (1986) used a linear 2-D time-dependent barotropic model, with 31 km resolution, to study pressure response to winter wind. A 120-day calculation was made, forced by observed subtidal pressure and observed wind products for the period. The mean circulation captured the two-gyre winter circulation with northward flow along the center axis as far inland as the Bohai Strait. Offshore pressure variation (i.e. the Kuroshio and Tsushima dynamics) dominated the response beyond the 100 m isobath but contributed less than 10% of the mean circulation in the Yellow and Bohai Seas.

Yanagi and Takahashi (1993) calculated a 3-D, 4-season climatology diagnostically, with a horizontal resolution of 50 km and three vertical layers. No-flow conditions across all wet boundaries prevented a correct interaction with the Kuroshio system. Summer results show cyclonic circulation in the top and middle layers, reversed at depth. In winter, a two-gyre structure was found, anticyclonic in the northern Yellow Sea and cyclonic to the south. Spring and autumn circulations were similar to winter. Yanagi et al. (1997) compared these results with geostrophic surface velocities estimated from Topex/Poseidon altimetry. They report qualitative agreement between altimetry-based and modeled surface circulation patterns; the altimetry-based speeds for summer were underestimated by the model.

Riedlinger and Preller (1995) applied the Princeton ocean model (3-D, prognostic, baroclinic) at 8 km resolution with 24 sigma levels. Care was taken to prescribe correct oceanic inflows; tidal forcing was neglected. A 14-month simulation for 1993 was initialized with January climatology. Seasonal variability was addressed by sampling the solution in March, June, September, and December. The basic winter circulation is captured in March and December: a northward warm current in the central Yellow Sea with southward flow along both coasts and coastally trapped Changjiang inflow. The summer results are more complex. The expected cyclonic circulation over the Yellow Sea Cold Water was not clearly developed. The summer Changjiang plume extended eastward toward Cheju Island.

2.2.3. Bohai

Zhao and Shi (1994) modeled the Bohai with a 3-D linear diagnostic model at $1/4^\circ$ horizontal resolution and level surfaces at 2.5 m spacing. Monthly averaged wind and hydrography were included; tidal forcing was neglected. Vertically averaged results show a cyclonic circulation originating in Bohai Strait in all seasons. In January (“winter”) this characterizes the entire Bohai; in June (“summer”) they report a two-gyre structure with anticyclonic circulation in Bohai Bay. The winter pattern is the result of wind-driven overturning, with surface flow uniformly to the south and deep return flow. The spring and fall patterns are weak, indicating that wind variability will dominate over the mean. The complex responses in all but the winter are poorly resolved.

Feng et al. (1994) report a similar 3-D diagnostic calculation of the Bohai during summer at a horizontal resolution of $1/6^\circ$. Driving forces included the tidal-rectifying force from a separate tidal model, in addition to wind and baroclinic forcing. Results without tidal rectification indicate

a single cyclonic gyre; tidal rectification added considerable detail in the bays, including an anticyclonic gyre in Bohai Bay and a pair of counter-rotating gyres in Liaodong Bay. It is concluded that the summer Bohai circulation is mainly due to tidal rectification, plus the inflow at Bohai Strait. The conflict between this finding and that of Zhao and Shi (1994) may arise in the boundary conditions at Bohai Strait.

Huang (1995) and Huang et al. (1999) applied the Hamburg Shelf model to the Bohai. This model is 3-D, baroclinic, prognostic, and tide-resolving. Horizontal resolution was $1/12^{\circ}$, with 10 vertical layers. The boundary was placed well seaward of Bohai Strait to avoid artifacts there. Tidal forcing included M2, N2, S2, O1, and K1. The RMS elevation errors for the M2 were 8 cm and 9°, based on a 29 station observational data set. The tidal residual velocity is generally 5 cm/s or less, with a prominent pair of headland gyres in northern Bohai Strait. The wind response is found to overwhelm the small tidal residual except at these headland gyres. An 8-month tidal simulation is reported in detail with observed atmospheric forcing; river inflow was neglected. The development and destruction of stratification is realistically portrayed and good agreement with sea surface temperature is shown. Cold water belts form on the mixed side of tidal mixing fronts. Circulation is generally cyclonic in the surface layer, and the deep circulation depends on the wind. Stratification is locally controlled by mixing and heat inputs. Strong inflow is found on the north side of Bohai Strait, and broad, weak outflow on the south side.

2.3. The present study

Modeling progress to date shows significant progress over the past two decades. Nevertheless a realistic simulation of the Yellow and Bohai Seas which includes adequate 3-D resolution and all processes affecting the subtidal circulation has not yet been made. Riedlinger and Preller's study comes the closest in this category, although tides and tidal mixing are lacking. Tidal models have become quite sophisticated, e.g. Kang et al. (1998) but generally have been limited to tidal phenomena only. Huang (1995) simulated a complete set of physical processes in 3-D, but the study was limited to the Bohai Sea.

This is the first comprehensive simulation of the Yellow and Bohai Seas which includes tides, atmospheric interactions, baroclinic forcing, and river input from the Changjiang. We force the Dartmouth Circulation Model, as specified in the next section, with seasonally dependent climatological values for wind, hydrography and Changjiang discharge, as well as seasonally invariant tides. The seasonal evolution of the circulation is captured by a series of six bimonthly calculations.

3. Procedure

3.1. Observational data products

The bathymetric depths for the Bohai, Yellow, and East China Seas (depths less than 200 m) are determined from a high-resolution data set distributed by C. Horton at NAVOCEANO in 1995. These data originated from South Korean sources and was compiled and processed by L.H. Kantha at the University of Colorado. The spatial resolution for this data is 5 min in longitude

and 4 min in latitude. For locations where depths exceed 200 m, bathymetry is derived from the NAVOCEANO Digital Bathymetric Data Base-5 min resolution (DBDB-5).

The bimonthly climatological hydrography is obtained from a preliminary release (July, 1997) of the MODAS 2.0 Synthetic Ocean Environment (Harding et al., 1998). This climatology was established utilizing data from 1920 to the present, from the US Navy's Master Oceanographic Observation Data Set (MOODS) (Bauer, 1982). It is output at 37 standard depths and a horizontal resolution of 0.125°. Our bimonthly estimates (January, March, May, July, September, and November) represent 3-month averages centered at the 15th of each respective month. Plots of surface and near-bottom properties for January ("winter") and July ("summer") appear in Figs. 3 and 4. In January, cold conditions prevail throughout, with minimal vertical structure. The salinity shows a bottom water intrusion of saline ECS water. This is the climatological signature of the Yellow Sea Warm Current. In July, the bottom salinity shows the accumulated impact of this wintertime intrusion and the Yellow Sea Cold Water is clearly evident in the deep waters, with thermal stratification of order 20°C. Hence, both temperature and salinity contribute to the density stratification of order $3\sigma_t$ for the central portion of the Yellow Sea, penetrating to near the Bohai Strait. Additionally, the reduced surface salinity near Shanghai indicates the eastward spreading of the Changjiang River discharge.

The wind stress climatology is taken from Hellerman and Rosenstein (1983). Their calculations were based upon surface observations obtained during the period 1870 through 1976 and a speed-dependent drag coefficient formulation (Bunker, 1976). Fig. 8 displays their data for our model domain at the horizontal resolution of the data set (2°). Strong northerly winds prevail during the winter, from November through March. The balance of the year, weaker winds are characteristic of the climatology. July is our representative "summer" season, with southerly winds. May and September are transition seasons.

Seasonal fresh water inputs from the Changjiang, taken from Riedlinger and Preller (1995) and listed in Table 1, are incorporated in the simulations. Monthly flow rates for the Changjiang vary from 9300 to $54,100\ m^3/s$, corresponding to January and July, respectively. As indicated previously, the Changjiang is the dominant river in the region, contributing approximately 90% of the composite inflow from the five major rivers in the region (Riedlinger and Preller, 1995).

The tidal station data set is based upon that compiled by Blain (1997), with minor modifications and a few additions. It consists of 121 sites throughout the Yellow and East China Seas having either tide gauge elevation observations or TOPEX/Poseidon derived sea surface heights. Tide gauges which have at least 180 days of record were extracted from the International Hydrographic Office database (IHO, 1979). Altimetric tides were derived from TOPEX data according to Desai and Wahr (1994).

3.2. Model

The 3-D finite element Dartmouth circulation model (Lynch et al., 1996) is our principal computational tool. This hydrostatic, free-surface model transports momentum, heat and salt, plus two turbulence variables, in tidal time on an f-plane. Variable horizontal resolution is provided on unstructured triangular meshes. A general terrain-following vertical coordinate allows smooth resolution of surface and bottom boundary layers. The baroclinic pressure gradient is evaluated on level surfaces to avoid generation of spurious motions on steep topography.

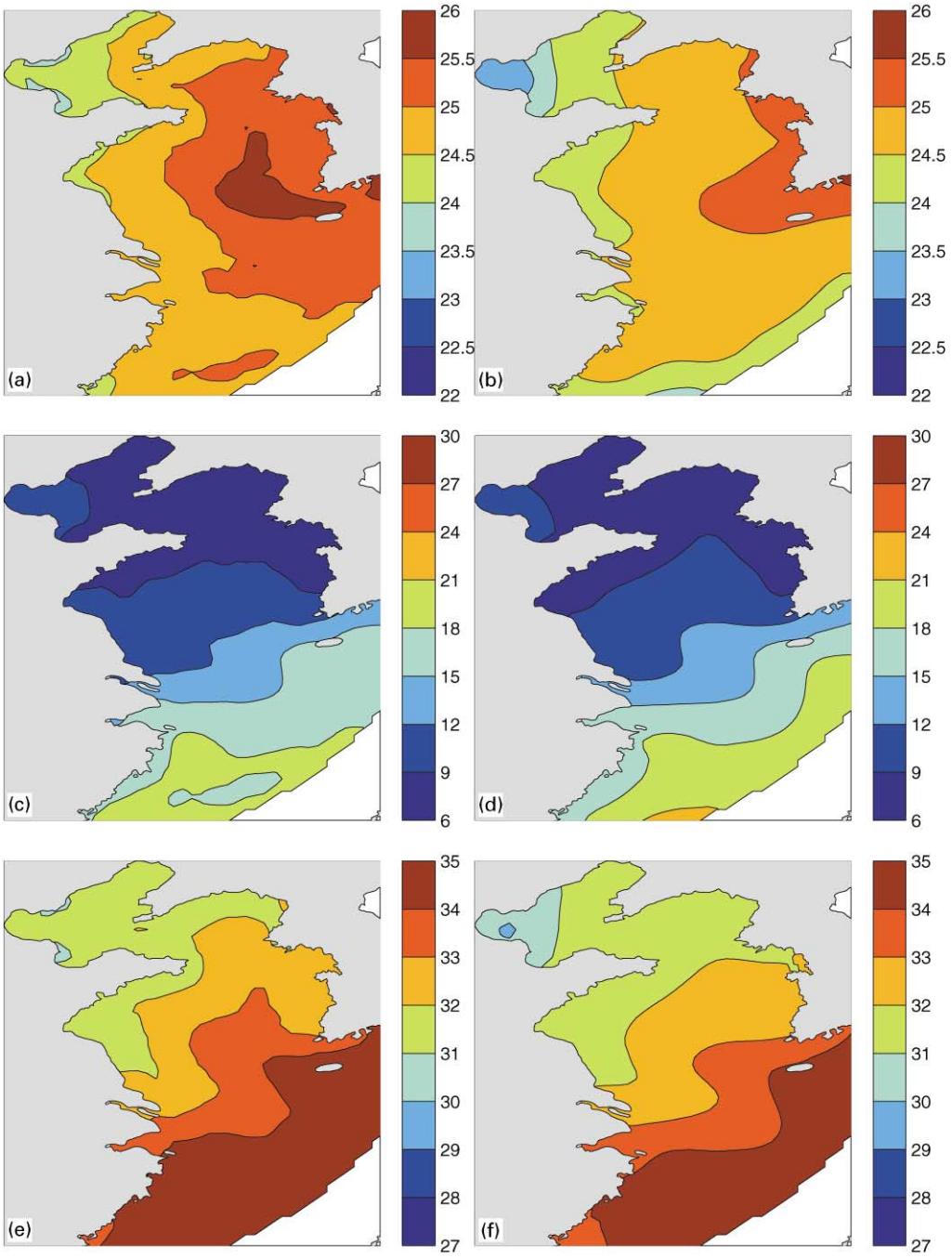

Fig. 3. January climatological hydrography: surface and near-bottom density (σ_t), temperature (°C), and salinity (PSU). (a) Bottom density; (b) surface density; (c) bottom temperature; (d) surface temperature; (e) bottom salinity; (f) surface salinity.

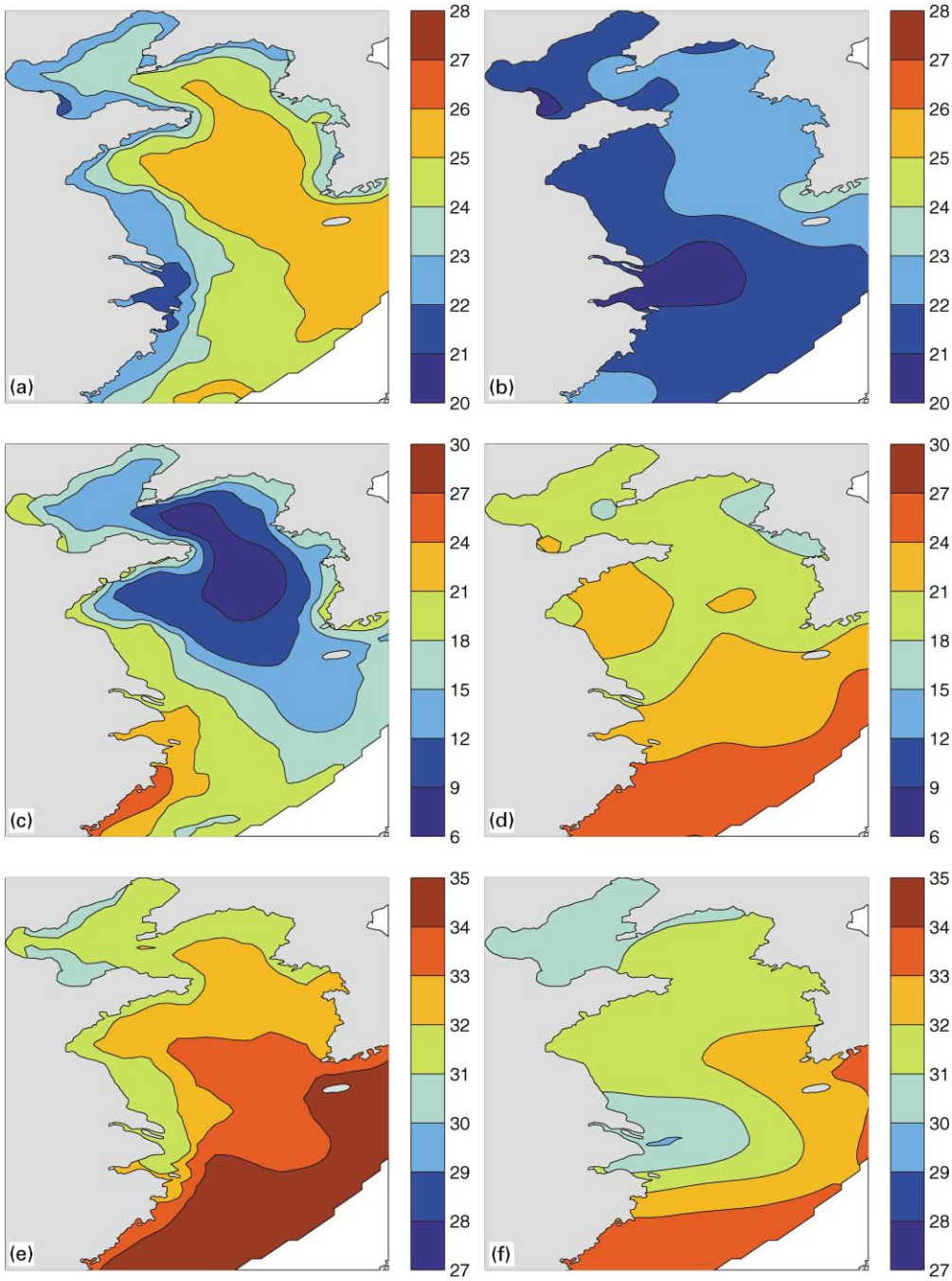

Fig. 4. July climatological hydrography: surface and near-bottom density (σ_t), temperature (°C), and salinity (PSU). (a) Bottom density; (b) surface density; (c) bottom temperature; (d) surface temperature; (e) bottom salinity; (f) surface salinity.

Table 1
Monthly discharge of Changjiang river into the Yellow Sea, from Riedlinger and Preller (1995)

Month	Input from Changjiang (10^3 m^3/s)
January	9.3
February	9.9
March	10.2
April	28.0
May	45.4
June	52.5
July	54.1
August	44.5
September	32.6
October	26.4
November	22.1
December	11.7

Vertical mixing is represented with a level 2.5 closure (Mellor and Yamada, 1982; Galperin et al., 1988; Blumberg et al., 1992). The model has been used extensively in the Gulf of Maine for similar purposes (Naimie, 1996; Lynch et al., 1997). Its use here parallels those studies and the model itself is essentially unchanged.

The computational mesh appears in Fig. 5. There are 9201 horizontal nodes, 17,111 triangles. Resolution is of order 8 km nearshore, and 32 km in the central Yellow Sea. In the vertical there are 20 elements everywhere, with 1 m resolution at the surface and bottom and a sinusoidal variation of Δz with depth.

3.3. Boundary conditions

At the seaward boundary, temperature and salinity were held constant at climatological values; while the sea surface elevation was specified as a composite of tidal and subtidal signals. The tidal elevation boundary condition components were obtained by inverting the aforementioned tidal observations using a procedure similar to that presented in Lynch et al. (1998) for tidal currents. This provided a least-squares fit of the linearized hydrodynamic model presented in Lynch et al. (1992) for each of the four constituents M2, S2, O1, K1. This calculation was performed on a wide-area mesh which extended into the ECS, with results then sampled at the boundary of the present mesh (Fig. 5).[1] These tidal contributions to the seaward boundary conditions were considered to be seasonally invariant. Seasonally varying contributions were added to represent the effects of wind and baroclinicity. The seasonal wind component was obtained from simulations on a larger-scale domain, forced

[1] The procedure revealed several difficulties in the tidal data and/or the bathymetry (e.g. areas with erratic spatial patterns of errors). Future studies may need to refine this tidal solution; it is sufficient for present purposes.

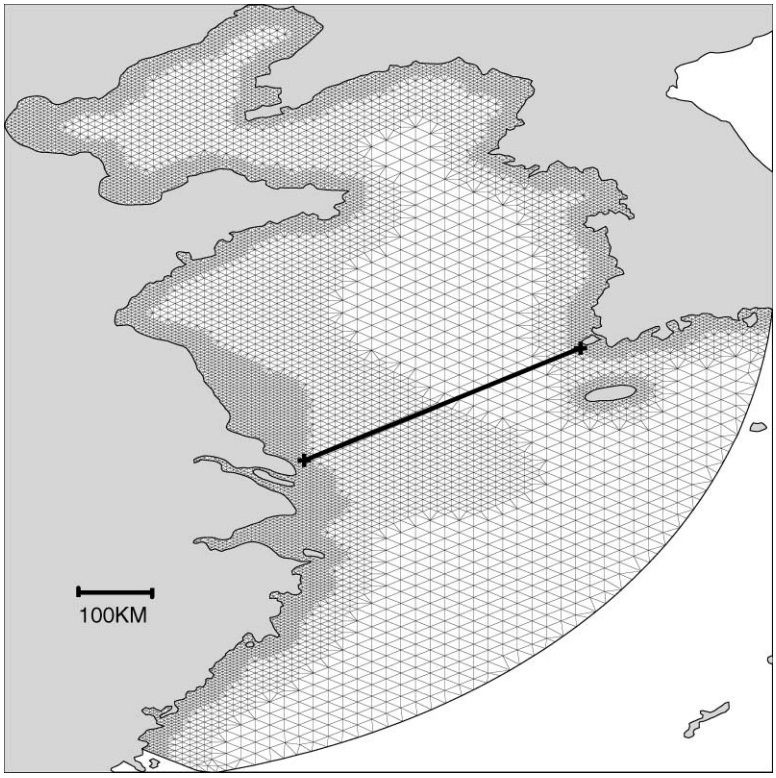

Fig. 5. Computational mesh: The bold line indicates the position of the transect used in the results section.

by Hellerman and Rosenstein (1983) seasonal winds alone. As above, we used the linearized model of Lynch et al. (1992) for these simulations and sampled the results along the seaward boundary of the present mesh. To this we added a signal based on the density field and calculated as in Naimie et al. (1994), to provide zero geostrophic bottom velocity normal to the boundary. We have found that this generally provides satisfactory transports at the seaward boundaries.

At the sea surface, the climatological wind stress was applied as the natural boundary condition for the momentum equation. Surface temperature was nudged to climatology (time scale 1 day) as a surrogate for the seasonal heating, and salt exchange was set to zero.

At the sea bed, we implemented a quadratic stress condition ($C_d = 0.005$) at a height of 1 m above the bottom. Within the context of the bottom stress parameterization, these selections dictate a roughness height of 0.0035 m (see Lynch et al., 1995). We also assumed there was no heat or salt exchange with the seabed.

At landward boundaries, conventional free-slip conditions were employed with no normal transport of heat, mass, or momentum. The Changjiang discharge was represented as a subtidal source of volume and buoyancy at ambient temperature.

3.4. Simulation procedure

Separate simulations were performed for each of six bimonthly periods (January, March, May, July, September, and November). In each case we initialized the simulation with climatological mass fields and a fluid at rest; ran diagnostically for 10 days with tidal forcing; activated the wind and the transport of heat and salt; and simulated for an additional 10 days. Solutions were sampled hourly over the final 9 days. These hourly samples were then fitted in the least-squares sense to a spectrum including the modeled tidal constituents and the mean circulation, using the tidal analysis packages of Foreman (1977, 1978).

As in previous studies (Naimie, 1996; Lynch et al., 1997), this procedure allows short-term prognostic adjustment of the climatological initial mass fields to tidal-time advection and mixing, facilitating the development of proper mixing fronts, the removal of database anomalies, and the sharpening of stratification features which are necessarily blurred in the climatology. However, the short-term simulation preserves the large-scale climatological signal due to river and oceanic inflows plus atmospheric heating, which is embedded in the mass field initialization. The calculation therefore could be characterized as diagnostic at interseasonal time scales, but prognostic at intraseasonal scales.

4. Results

4.1. Tidal response

The January tidal elevation response is displayed in Fig. 6. The basic 4-amphidrome semidiurnal system noted in previous studies (e.g. Choi, 1980; Kang et al., 1998) is reproduced for the M2 and S2 constituents, while the K1 and O1 exhibit a structure consistent with the 2-amphidrome diurnal structure in Kang et al. (1998). Our results also agree with Kang et al. (1998) in the context of the sense of rotation for the M2 and K1 currents. While we do find subtle shifts in the tidal amplitude and current responses for the various seasons, they are small relative to the strength of the signals.

Our principal interests in the tidal response are the associated contributions to vertical mixing (via bottom-generated turbulence) and the residual circulation (via tidal rectification). Both are likely to illustrate seasonal dependence, especially the residual circulation which can be more sensitive to friction than the tide itself. Relative to vertical mixing, the Simpson and Hunter (1974) mixing parameter is plotted in Fig. 7 for the January simulation. Considering the 10^2 contour to represent the potential location for the tidal mixing front, we expect tidally mixed regions along the Korean coast, along the Chinese coast south of the Shangdong peninsula and extending well offshore of Shanghai, and localized areas in the Bohai. These results are very similar to those reported by Lie (1989), which were based on a 2-D solution. Examination of similar results to those presented in Fig. 7 for the remainder of our seasonal simulations (not displayed herein) indicates that the model-predicted patterns of tidal mixing are nearly invariant over the year in the Yellow Sea proper; while localized details in the Bohai Sea show some seasonal dependence.

The contribution of tidal rectification to the subtidal circulation is discussed below, in conjunction with the discussion of the relative importance of other modeled processes.

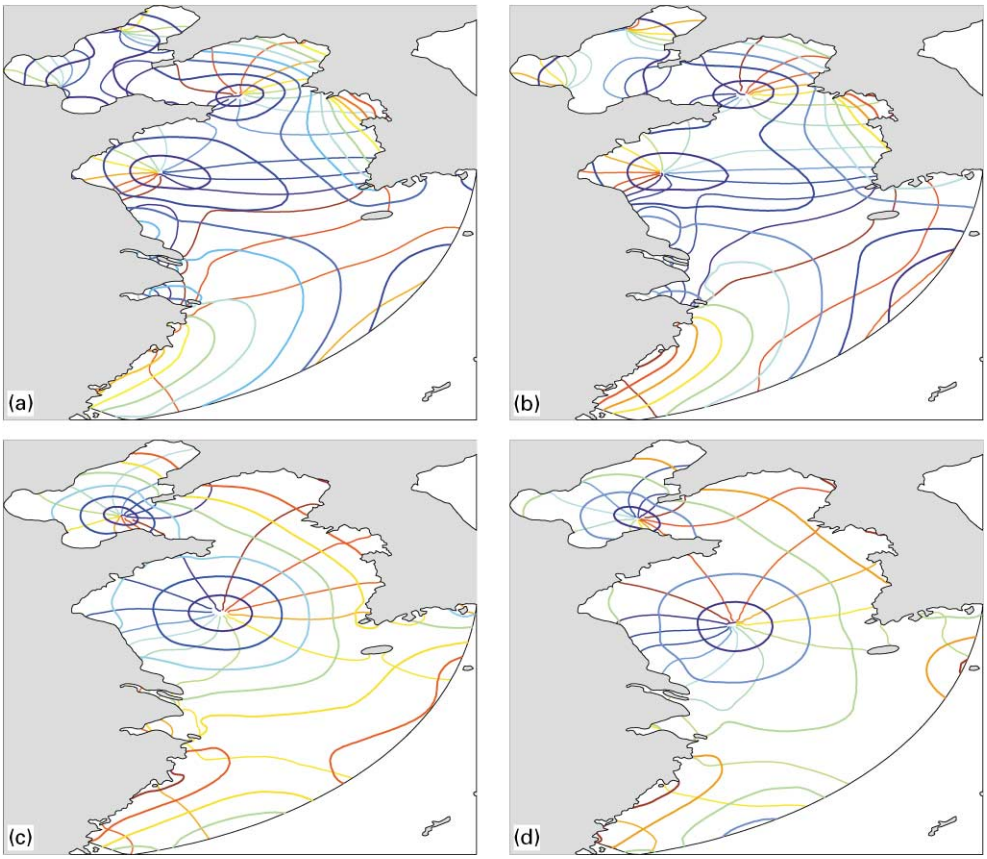

Fig. 6. January solution: M2, S2, O1, and K1 tidal constituents. (a) M2: 25/0 (blue) to 275/330 (red) by 25/30 [cm/deg]. (b) S2: 10/0 (blue) to 90/330 (red) by 10/30 [cm/deg]. (c) K1: 5/0 (blue) to 35/330 (red) by 5/30 [cm/deg]. (d) O1: 5/0 (blue) to 25/330 (red) by 5/30 [cm/deg].

4.2. Subtidal circulation

Fig. 8 displays the vertically averaged bimonthly subtidal circulation. Also included in this figure are vectors of the Hellerman and Rosenstein (1983) climatological wind stress, on their original grid.

May provides a reasonable starting point for a discussion of the seasonal subtidal circulation features, as it exhibits the least complicated circulation pattern. The most prominent feature is northeastward flow along the ECS shelf. This intense flow is the Taiwan Warm Current (TWC in Fig. 2). The inner edge of the TWC follows the 40 m isobath in the western ECS and turns east at the boundary of the ECS and the Yellow Sea. Bathymetric steering is also apparent along the deeper bathymetric contours, especially south of Cheju Island where the current turns due north. The Changjiang River Plume (CRP in Fig. 2) flows eastward toward Cheju Island, at the northern edge of the TWC. In the region south of Korea, the TWC supplies the Tsushima Current (TC in Fig. 2) which continues eastward through the Korean Strait. The circulation in the Yellow Sea is very weak, with no distinct features at the scales displayed herein.

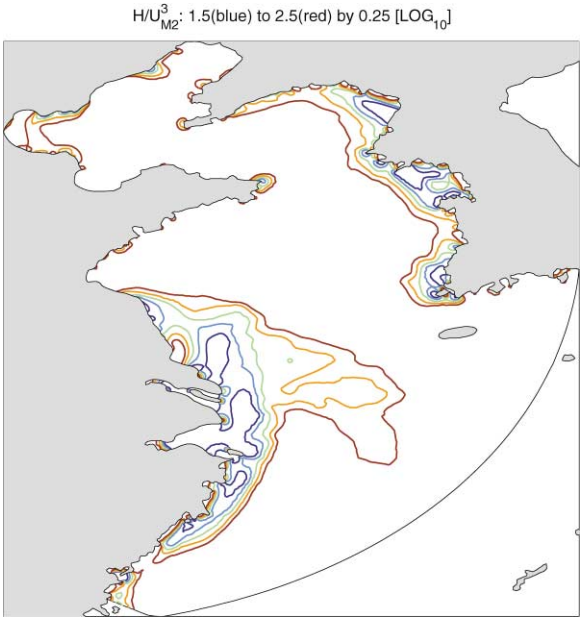

Fig. 7. January solution: Simpson–Hunter parameter (H/U^3), plotted on a base-10 logarithmic scale for the M2 response.

July circulation features in the ECS are very similar to those for May, with a general tendency for intensification. An exception is along the southern coast of China, where the northward flow of the East China Sea Coastal Current has been established (ECSCC in Fig. 2). In the Yellow Sea, a 0.2 Sv cyclonic gyre has emerged over the Yellow Sea Cold Water (YSCW; recall Fig. 4). There is also a northward flow in the shallow regions along the Chinese coastal regions of Jaingsu, a small anticyclonic gyre at the tip of Shangdong Peninsula, and weak circulation features in the Bohai Sea. As for May, the Changjiang discharge flows eastward.

The September solution indicates some important dynamical differences with respect to that displayed in July. The TWC does not penetrate as far northward and inshore of the TWC the ECSCC has reversed. While the TC continues to flow eastward in the Korean Strait, a flow reversal has occurred north of Cheju Island. Furthermore, the cyclonic gyre associated with the YSCW has expanded in geographical context and intensified to nearly 0.3 Sv. The Changjiang discharge is bimodal with a portion flowing eastward as in the May/July and a portion joining the ECSCC and flowing to the southwest along the coast of China.

During November, the TWC is not present as a coherent northeastward circulation feature within the model domain, though we still see its influence south of Korea. The dominant Yellow Sea circulation feature during July and August, the cyclonic Yellow Sea Gyre, has been replaced by two counter-rotating gyres in November. Other small-scale circulation features are also emerging in the Yellow Sea as winter sets in. The weaker Changjiang input still appears bimodal, with both eastward and southwestward tendencies.

By January, we find no signature of the TWC within the model domain. This appears to be the result of two effects. First, the southward ECSCC dominates the circulation in the southwest

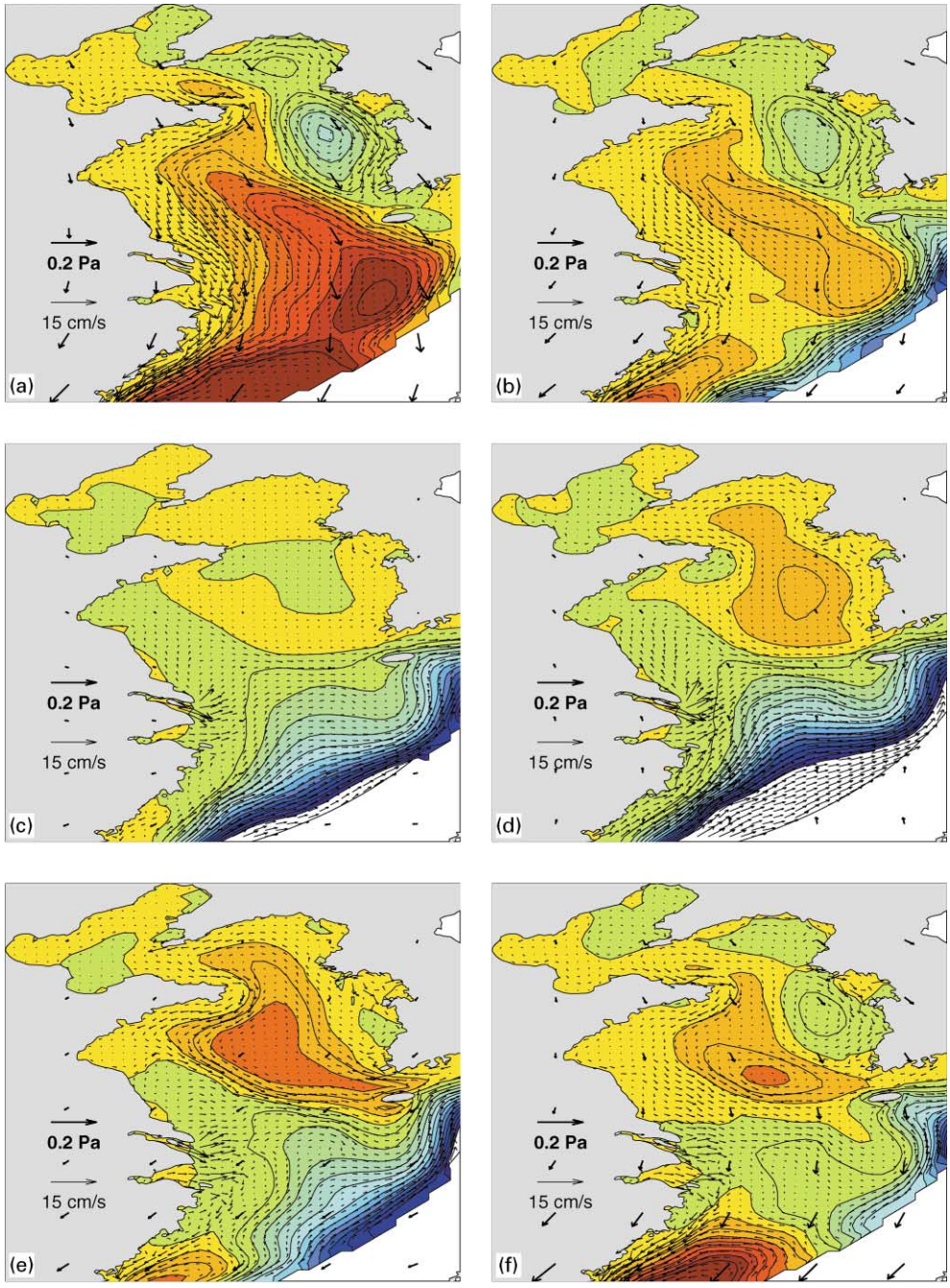

Fig. 8. Annual cycle: Hellerman and Rosenstein (1983) wind stress (heavy vectors, plotted at the spatial resolution (2.0°) of the data); model predicted vertically averaged residual velocity (thin vectors, interpolated to a 0.25° grid for display purposes in this and subsequent figures); and the associated stream function (increasing from blue to red in 0.05 Sv increments; circulation around local minima is anticyclonic). (a) January; (b) March; (c) May; (d) July; (e) September; (f) November.

corner of the model domain. Second, flow entering the model domain near the center of the open boundary supplies a northward flow exceeding 0.4 Sv in the trough connecting the East China and Yellow Seas instead of supplying the TC. This second effect signifies the emergence of the Yellow Sea Warm Current (YSWC in Fig. 2). Along the Chinese and Korean coasts, we find coherent southward flow in the Yellow Sea Coastal Current (YSCC in Fig. 2) and the Korean Coastal Current (KCC in Fig. 2), respectively. The combination of the northward YSWC and the southward YSCC result in the breakdown of the cyclonic Yellow Sea Gyre into a loop current which penetrates from the ESC shelf past Shangdong Peninsula into the Bohai Sea. East of this loop current, the anticyclonic gyre noted in the November solution has intensified to over 0.4 Sv due to its location between the YSWC and the KCC and a second weaker cyclonic gyre is evident in Seahan Bay. Finally we note that the weak CRP flows southward, trapped tightly against the coast.

In the March solution, we note that the TWC is reestablished as a coherent northeastward shelf current along the boundary of the model domain. The circulation pathway for northward penetration of the YSWC through the ECS and into the Yellow Sea is very similar to that for January, though the intensity is reduced to approximately 0.2 Sv and the flow does not penetrate as far north. The combination of the YSWC and the YSCC create an elongated cyclonic gyre over the Yellow and East China Seas. As in November and January, there is an anticyclonic gyre east of Kyunggi Bay which reflects the interaction of the YSWC and the KCC. Similar to January, subtidal flow from the Changjiang and out of Hangzhou Bay are entrained in the southward YSCC. As for all other periods except January, we find a relatively isolated set of circulation features in the Bohai, with velocities on the order of a few cm/s.

While this description of the vertically integrated circulation is instructive regarding the prominent circulation features, further analysis related to process partitioning of the dynamics and examination of the vertical structure is warranted. Indeed, some of the circulation "features" just discussed result from the vertical averaging of dramatically different near-surface and deep circulation patterns. This is particularly evident from the bimonthly subtidal circulation results displayed in Fig. 9, for a plane from Shanghai to Cheju Strait (see Fig. 5). This section highlights the dominant winter and summer modes. The winter circulation (January and March) is nearly barotropic with southward flow along the coasts and northward flow over the central trough. The cyclonic Yellow Sea Gyre begins to develop in May; though the dominant summer mode, consisting of the cyclonic Yellow Sea Gyre and northeastward circulation (i.e. along the transect) consistent with the summer intrusion of the TWC, does not reach full strength until September. Through the summer, the circulation on the Chinese shelf remains mostly barotropic, though complex circulation features are apparent over the central trough and near Korea.

We now proceed with a more thorough discussion of process partitioning and the vertical structure of the circulation, by focusing on the seasonal extremes of the winter and summer circulation.

4.2.1. Winter

Fig. 10 provides an approximate dynamic partitioning among the processes modeled: barotropic tidal rectification, baroclinic pressure gradients, wind, and Changjiang River discharge. Our strategy for determining the contributions from various processes consists of performing a series of numerical simulations, adding one process for each step along the way.

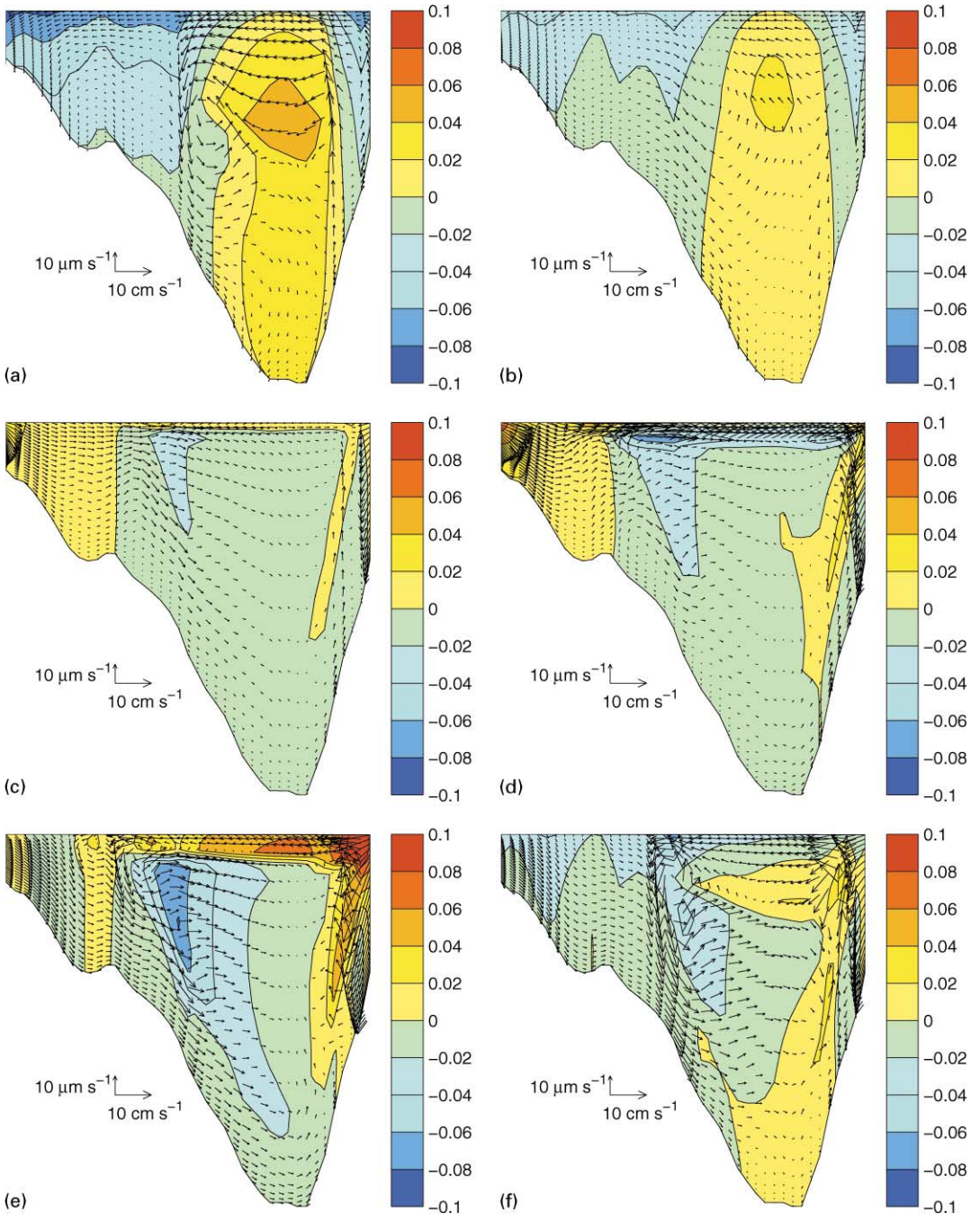

Fig. 9. Annual cycle: Exchange between the Yellow and East China Seas. Plotted are contours (vectors) of velocity normal (tangent) to the transect indicated in Fig. 5. Positive normal velocity is northward (i.e. into the page). (a) January; (b) March; (c) May; (d) July; (e) September; (f) November.

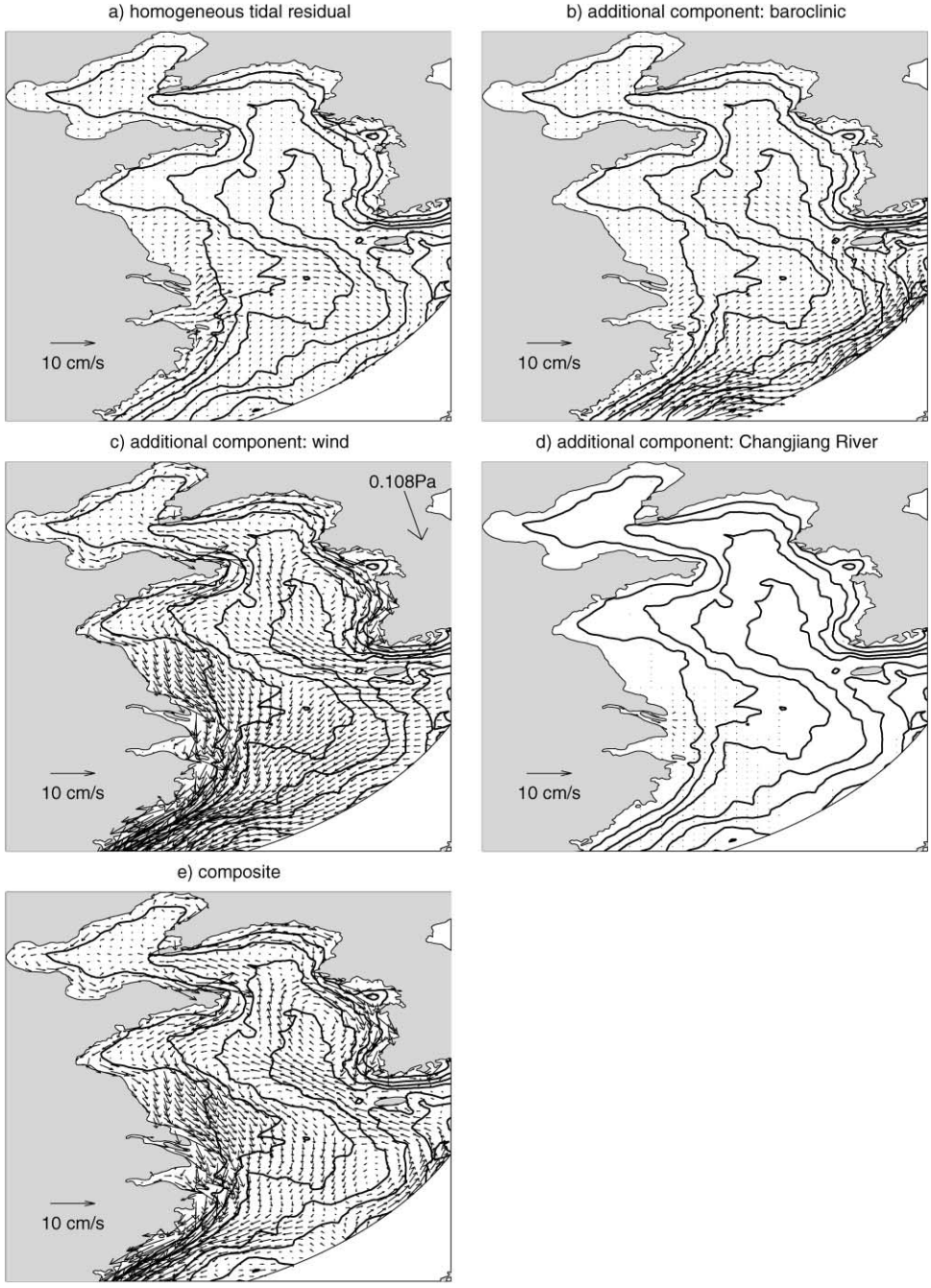

Fig. 10. January residual circulation: Approximate dynamical partitioning of vertically integrated circulation. The "Composite" circulation (panel e) is the climatological mean for January (i.e. it is identical Fig. 8a). This composite is the sum of the individual contributions from barotropic tidal rectification (panel a), baroclinic processes (panel b), wind (panel c), and the Changjiang River (panel d).

Then we approximate the contribution of a particular process by evaluating the difference between the solutions before and after that process was added. Our first solution in this cascade is the barotropic tidal solution.[2] Hence, the only generating mechanism for the subtidal circulation is barotropic tidal rectification. The remaining processes are added in the order listed above. First, we add the baroclinic forcing and conduct a prognostic simulation to evaluate the contributions from baroclinic processes.[3] Next, we include wind forcing. Finally, we include discharge from the Changjiang River. We also include a "Composite" panel which displays the complete solution.

Comparing results from the individual panels in Fig. 10 clearly indicates that, of the processes modeled, the wind is the dominant dynamical process in the Yellow Sea during January. The baroclinic TWC (panel b) flows to the northeast along the shelf break, turns north along the bathymetric trough, and turns back east to exit the domain on both sides of Cheju Island. However this large-scale baroclinic signal is overwhelmed by the wind influence in the region south of China. The result is a mean flow of the YSCC, CRP, and ECSCC to the southeast and an apparent breakdown of the TWC and/or its migration seaward of our boundary. Off-shore of Shanghai, we find a relatively broad tidally rectified eastward flow of a few cm s^{-1} along with very local and weak response to the Changjiang River. Finally, we note a baroclinic cyclonic gyre near the center of the model domain, the complicated but weak wind response of the Bohai, and the prominence of the wind-driven KCC. To examine further the vertical structure of the January circulation, we consider the circulation for a vertical transect from Shanghai to Cheju Strait (Fig. 9), along with the near-bottom and near-surface circulation for the entire model domain (Fig. 11). Considering first the vertical transect results, we find southward coastal currents with near-surface speeds in excess of 6 cm s^{-1} in the shallow regions along both the Chinese and Korean coasts (the YSCC and KCC), southwestward Ekman drift of a few cm s^{-1} over the center of the along-axis channel which runs from the ECS to the Yellow Sea, and a deep northward return flow within this same channel (the YSWC), which achieves a maximum speed exceeding 5 cm s^{-1} at a depth of 30 m. The results displayed in Fig. 11 illustrate that these phenomena represent the large-scale flow in the entire Yellow Sea. Over the center of the Yellow Sea and the deep region of ECS, the surface layer flows uniformly to the southwest. In the shallow regions near both the Chinese and Korean coasts, intense vertical mixing results in the YSCC and KCC's penetration to the bottom of the water column. Compensating these transports is the strong return flow of the YSWC in the deep central region of the Yellow Sea. At Shangdong Peninsula, the YSWC partly upwells along both China and Korea coasts. The remainder penetrates further toward the Bohai Sea. At Liaodung Peninsula, most of the remaining flow upwells and is deflected eastward, feeding the KCC north of Seahan Bay. Generally, we have wind-driven coastal currents along all coasts, draining the Bohai and Yellow Seas, with return flow beneath the Ekman layer in the deepest areas. Coherent northeastward flow of the TWC is not apparent within the domain considered, due to the cancellation of baroclinic circulation by the wind-driven flow discussed previously.

[2] Conducting the tidal simulation first is important to ensure the effects of tidal mixing will be included in all simulations.

[3] One of the aspects which makes the results presented herein approximate is that the addition of new processes will affect contributions from other processes. An example of this phenomenon is the impact of stratification on vertical mixing which may alter the tidal rectification.

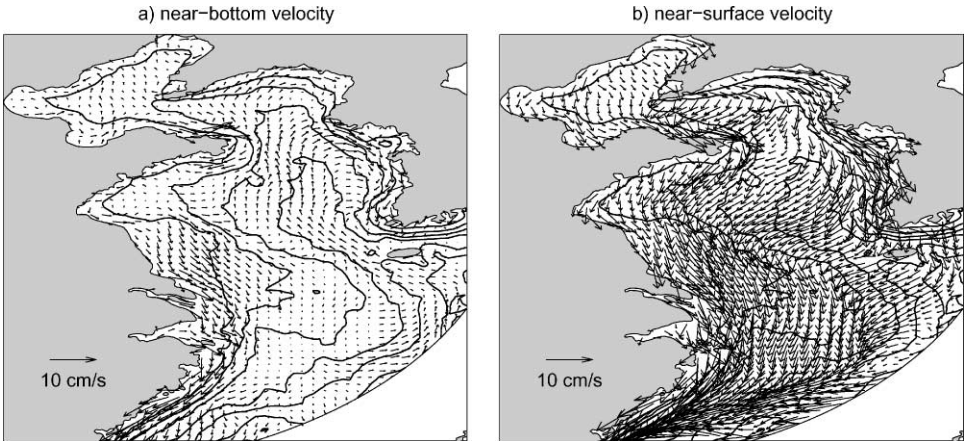

Fig. 11. January residual circulation: (a) near-bottom and; (b) near-surface horizontal velocity.

The circulation in March exhibits the same general structure as January, though the reduced wind forcing has two important effects. First, it facilitates the TWC's emergence as a coherent northeastward flow at the seaward boundary of the study area (unlike January, the wind is not strong enough to overwhelm the baroclinic forcing). Second, it reduces the intensity of the YSWC to approximately half that predicted for January (Fig. 9).

4.2.2. Spring transition

May is quiescent over much of the domain. The most noteworthy circulation features are the eastward Changjiang discharge and the well-established TWC. Over the deeper regions of the Yellow Sea, the weak wind response opposes the weak baroclinic cyclonic gyre.

4.2.3. Summer

Approximate process partitioning results for the July solution are determined in a manner analogous to that presented earlier for the January solution. As displayed in Fig. 12, the baroclinic forcing dominates the summer scenario in both the Yellow and East China Seas. Over the western Yellow Sea, a 0.2 Sv cyclonic gyre encompasses the entire deep basin. This is the baroclinic response to the Yellow Sea Cold Water. The TWC is a well-established feature over the ECS, forced mainly by baroclinic pressure gradients with an additional contribution from the wind-driven response to the south wind. The northward wind-driven circulation on the Chinese coastline dominates the nearshore circulation off Jiangsu and opposes the western limb of the Yellow Sea Gyre. This results in a more complicated circulation scenario than that discussed in Su (1998). However, the northward wind-driven KCC along the Korean Coast reinforces the eastern limb of the Yellow Sea Gyre discussed above. As discussed for the winter solution, the major circulation feature forced by the homogeneous tidal residual is an eastward flow near Shanghai. The peak vertically averaged velocities correspond to river discharge from the Changjiang, reaching nearly 10 cm/s near the river mouth. These tidally rectified and river-forced phenomena are driven eastward in the CRP by the joint influences of the TWC, the Yellow Sea Gyre, and the

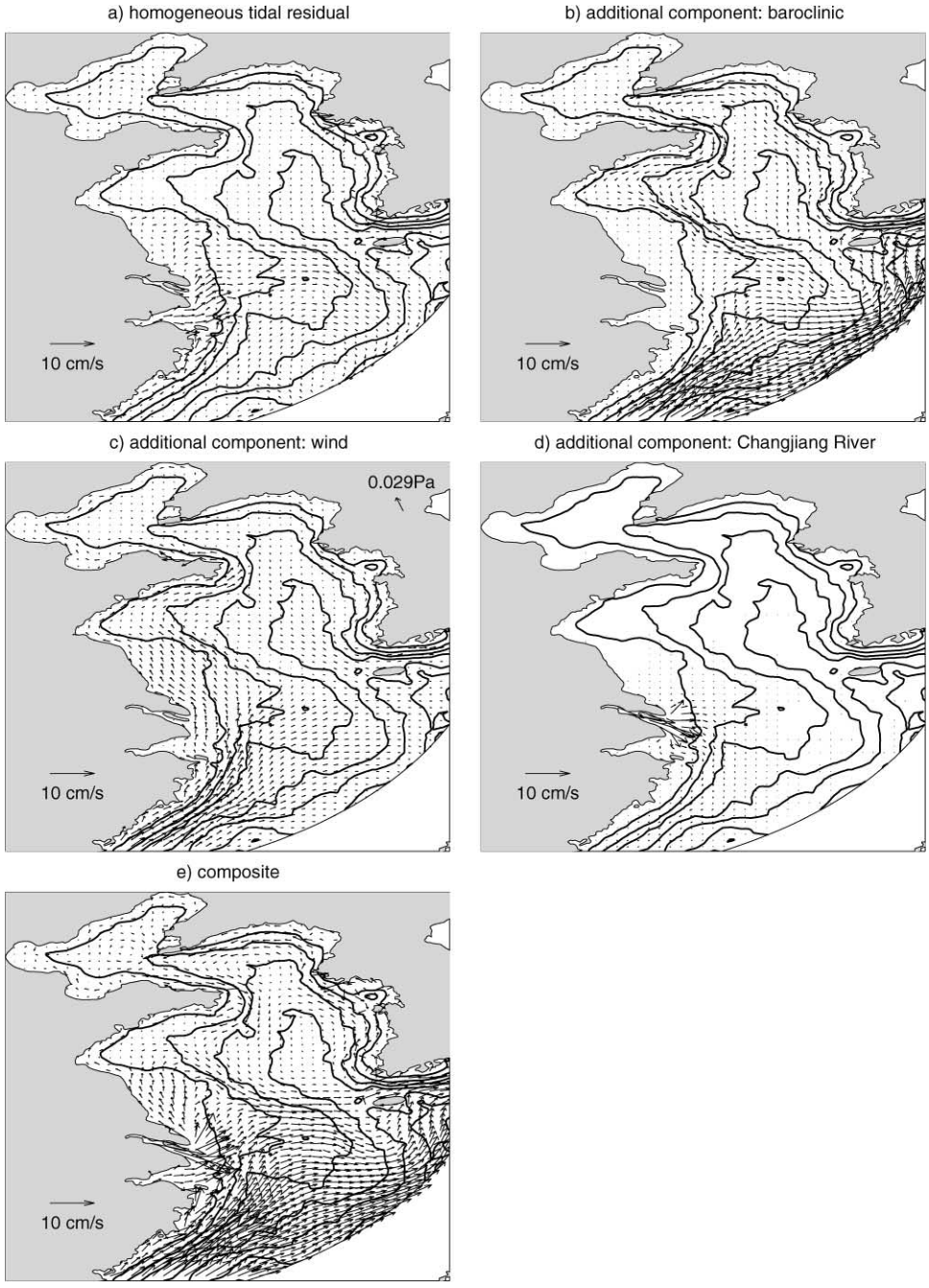

Fig. 12. July residual circulation: approximate dynamical partitioning of vertically integrated circulation. Same conventions as Fig. 10.

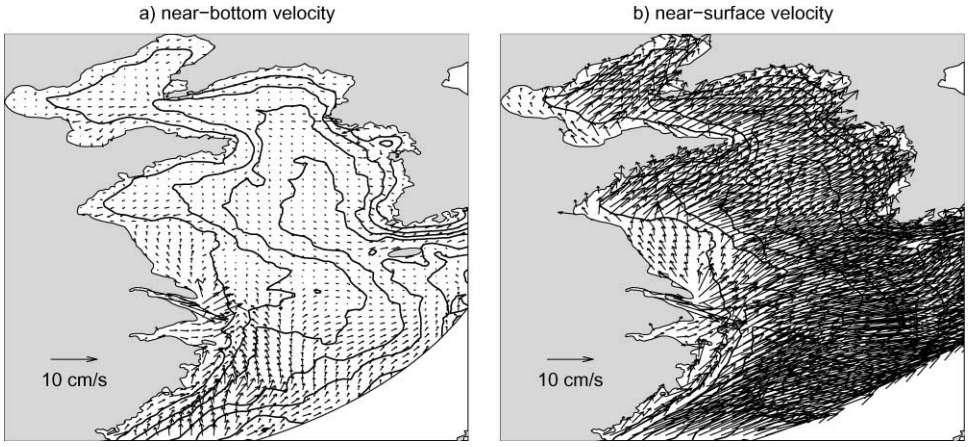

Fig. 13. July residual circulation: (a) near-bottom and; (b) near-surface horizontal velocity.

weak summer winds. The Bohai is complex, with several small recirculating features and limited exchange with the Yellow Sea.

The results displayed for the vertical transect from Shanghai to Cheju Island (Fig. 9) reinforce points made above regarding the exchange between the Yellow and East China Seas. A northward wind-driven coastal current is seen along the Chinese coast. There is a thin Ekman layer flowing towards the northeast over the baroclinic response to the Yellow Sea Cold Pool, and eastward flow near the Changjiang discharge. The near-bottom and near-surface velocity fields displayed in Fig. 13 further corroborate the aforementioned circulation features.

September exhibits a similar baroclinic mode to July, but the shifted winds (now northeasterly) result in significant differences in the response over the central Yellow Sea and the ECS. The major features are shifted to the west.

4.2.4. Fall transition

By November, the characteristic winter wind forcing is reestablished but the YSWC is not fully developed. The net result is a complicated interaction between the Yellow and East China Seas, as illustrated in Figs. 8 and 9. While winter-time circulation features are emerging, the Yellow Sea is predominately in transition between two very active dynamical modes.

5. Summary and conclusion

The three-dimensional climatological circulation has been computed for the Yellow and Bohai Seas in a series of six bimonthly realizations. The model is nonlinear, tide-resolving, and baroclinic with advanced turbulence closure. Resolution approaches 8 km in nearshore areas. Data inputs include seasonal hydrography, seasonal mean winds, seasonal mean discharge from the Changjiang, and seasonally invariant oceanic tides.

Results for winter and summer exhibit two distinct circulation modes. In winter, strong northerly wind drives southward flow at the surface and along both Korean and Chinese coasts.

This is compensated by deep return flow — the YSWC — in the central trough of the Yellow Sea, penetrating to the Bohai. The Changjiang discharge exits to the southwest in winter, trapped along the Chinese coast. The Taiwan Warm Current is outside the domain of the model, as the baroclinic tendency within the model domain is overwhelmed by the wind.

In summer, the cold water pool produced by winter cooling — the YSCW — is isolated in the deep trough, setting up cyclonic circulation over the eastern Yellow Sea. Summer winds from the south drive northward and eastward flow along the Chinese coast. The composite summer result is a qualitative reversal of the winter pattern. The Changjiang discharge is driven offshore toward the Korean Strait by the summer wind. Reinforcing this is a strong Taiwan Warm Current which enters the domain from the west, loops northward along the Chinese shelf, then generally traverses along-shelf toward the Korean Strait.

Relative to previous model results, we find general agreement for Winter. The basic wind-driven mode is very robust and has shown up in much simpler models. Our results elaborate this mode and provide enhanced local detail. The concensus Winter map of Su (1998) (Fig. 2a herein) is essentially correct in terms of major features and dynamics. The summer circulation has been more problematic for modelers. There has been reasonable agreement on the presence of a cyclonic gyre over the deep eastern basin, and we confirm this. However we find this feature coexists with a wind-driven mode in the western Yellow Sea, resulting in northeastward transport west of the gyre. In this aspect, the concensus drawing of Su (1998) (Fig. 2b herein) is too coarse, and the solutions here represent an advance. They deserve experimental verification, and continued studies at higher resolution are certainly desirable.

The winter and summer circulations are partitioned dynamically among responses to tidal rectification, baroclinic processes, wind, and Changjiang River discharge. Wind dominates the winter pattern. In summer, the baroclinic processes dominate the eastern Yellow Sea; while all of the remaining processes make significant contributions to the circulation in the western Yellow Sea.

The seasonal cycle indicates that January and March exhibit the same basic winter pattern. May is quiescent, followed by July which defines the summer mode. September shows the same general summer pattern, with features shifted westward. November is a transition period followed by winter conditions.

The pictures and discussion presented herein are far from a complete description of the six 3-D fields, and many features deserve more detailed scrutiny. To facilitate this, we have archived the solutions electronically (Naimie and Lynch, 1999). In addition to extending the general kinematic and dynamic analyses herein, we anticipate several uses of these solutions:

- as a guide to field programs,
- as a best prior estimate for data-assimilative hindcasting and forecasting models,
- as a vehicle for studying fate and transport of marine materials and plankton.

Uses in the last category can be very productive. For example we have carried out several ecological studies in the Gulf of Maine wherein growth, development, behavior, and reproduction of planktonic animals are computed along Lagrangian pathways (Lynch, 1999). Care must be used, however, in posing and interpreting these studies with climatological mean fields, without a companion description of variability. We look forward to future developments in this area, as well as to future refinements to the mean fields presented here.

Acknowledgements

This work was sponsored by the U.S. Office of Naval Research, grant Number N00014-96-1-0572. We thank Ruth Preller for several helpful discussions, Charlie Horton and Lakshmi Kantha for the high-resolution bathymetric database, as well as John Harding and colleagues for the hydrographic data.

References

An, H.S., 1977. A numerical experiment of the M2 tide in the Yellow Sea. Journal of the Oceanographical Society of Japan 33, 103–110.

Bauer, R., 1982. Functional description: Master Oceanographic Observation Data Set (MOODS). Compass Systems Inc.

Blain, C.A., 1996. An evaluation of tidal predictions in the Yellow and East China Seas. In: Spaulding, M.L., Cheng, R.T. (Eds.), Estuarine and Coastal Modeling. Proceedings of the 4th International Conference. ASCE, pp. 429–441.

Blain, C.A., 1997. Development of a data sampling strategy for semienclosed seas using a shallow-water model. Journal of Atmospheric and Oceanic Technology 14, 1157–1173.

Blumberg, A.F., Galperin, B., O'Connor, D.J., 1992. Modeling vertical structure of open-channel flows. ASCE Journal of Hydraulic Engineering 118, 1119–1134.

Bunker, A.F., 1976. Computations of surface energy flux and annual air-sea interaction cycles of the North Atlantic Ocean. Monthly Weather Review 104, 1122–1140.

Chao, S.-Y., 1991. Circulation of the East China Sea, a numerical model. Journal of the Oceanographical Society of Japan 46, 273–295.

Choi, B.H., 1980. A tidal model of the Yellow Sea and the Eastern China Sea. Korea Ocean Research and Development Institute (KORDI) Report 80-02, 72 pp.

Choi, B.H., 1984. A three-dimensional model of the East China Sea. In: Ichiye, T. (Ed.), Ocean Hydrodynamics of the Japan and East China Seas, Oceanography Series, Vol. 39. Elsevier, Amsterdam, pp. 209–224.

Choi, B.H., 1990. A fine-grid three-dimensional M2 tidal model of the East China Sea. In: Davies, A.M. (Ed.), Modeling Marine Systems, Vol. 1. CRC Press, Boca Raton, FL, pp. 167–185.

Desai, S.D., Wahr, J.M., 1994. Another ocean tide model derived from TOPEX/POSEIDON satellite altimetry (abstract). EOS 75, 57.

Dou, Z., Yang, L., Ozer, J., 1994. Numerical simulation of three-dimensional tidal current in the Bohai Sea. Acta Oceanologica Sinica 13 (2), 155–172.

Fang, G.-h., 1994. Tides and tidal currents in East China Sea, Huanghai Sea and Bohai Sea. In: Zhou, D., et al. (Ed.), Oceanology of China Seas, Vol. 1. Kluwer Academic Publishers, Dordrecht, pp. 101–112.

Feng, S.-z., Zhang, S.-Z., Xi,, P.G., 1994. A Lagrangian model of circulation in Bohai Sea. In: Zhou, D., et al. (Ed.), Oceanology of China Seas, Vol. 1. Kluwer Academic Publishers, Dordrecht, pp. 83–89.

Foreman, M.G.G., 1977. Manual for tidal heights analysis and prediction. Pacific Marine Science Report 77-10, Institute of Ocean Sciences, Patricia Bay, Sidney, BC.

Foreman, M.G.G., 1978. Manual for tidal currents analysis and prediction. Pacific Marine Science Report 78-6, Institute of Ocean Sciences, Patricia Bay, Sidney, BC.

Galperin, B., Kantha, L.H., Hassid, S., Rosati, A., 1988. A quasi-equilibrium turbulent energy model for geophysical flows. Journal of Atmospheric Science 45, 55–62.

Guan, B.-x., 1994. Patterns and structures of the currents in Bohai, Huanghai and East China Seas. In: Zhou, D., et al. (Ed.), Oceanology of China Seas, Vol. 1.. Kluwer Academic Publishers, Dordrecht, pp. 17–26.

Harding, J., Preller, R., Rhodes, R., 1998. Coastal ocean prediction at the Naval Research Laboratory. In Proceedings of the 2nd Conference on Coastal and Oceanic Prediction and Processes, 11–16 January, 1998, Phoenix, AZ. American Meteorological Society, pp. 108–114.

Hellerman, S., Rosenstein, M., 1983. Normal monthly wind stress over the world ocean with error estimates. Journal of Physical Oceanography 13 (7), 1093–1104.

Hsueh, Y., Romea, R.D., DeWitt, P.W., 1986. Wintertime winds and coastal sea-level fluctuations in the Northeast China Sea. Part II: Numerical Model. Journal of Physical Oceanography 16, 241–261.

Hu, D.X., 1994. Some striking features of circulation in Huanghai Sea and East China Sea. In: Zhou, D., et al. (Ed.), Oceanology of China Seas, Vol. 1. Kluwer Academic Publishers, Dordrecht, pp. 27–38.

Huang, Z.K., 1991. Tidal waves in Bohai Sea and their variations. Journal of Ocean University of Qingdao 21 (2), 1–12.

Huang, D., 1995. Modelling studies of barotropic and baroclinic dynamics in the Bohai Sea. Thesis, Institut fur Meereskunde, Universitat Hamburg.

Huang, D., Su, J., Backhaus, J.O., 1999. Modelling the seasonal thermal stratification and baroclinic circulation in the Bohai Sea. Continental Shelf Research 19, 1485–1505.

IHO, 1979. Tidal constituent bank station catalogue. International Hydrographic Organization, Canadian Hydrographic Service, Ottawa, ON, K1A OE6 Canada.

Kang, S.K., Lee, S.-R., Yum, K.-D., 1991. Tidal computation of the East China Sea, the Yellow Sea and the East Sea. In: Takano, K. (Ed.), Oceanography of Asian Marginal Seas, Oceanography Series, Vol. 54. Elsevier, Amsterdam, pp. 25–48.

Kang, S.K., Lee, S.R., Lei, H.J., 1998. Fine grid tidal modeling of the yellow and east china seas. Continental Shelf Research 18 (7), 739–772.

Kantha, L.H., 1995. Barotropic tides in the global oceans from a nonlinear tidal model assimilating altimetric tides 1. Model description and result. Journal of Geophysical Research 100, 25,283–25,308.

Kantha, L.H., Bang, I., Choi, J., Suk, M., 1996. Shallow water tides in the seas around Korea. The Journal of the Korean Society of Oceanography 31 (3), 123–133.

Larsen, L.H., Cannon, C.A., Choi, B.H., 1985. East China Sea tide currents. Continental Shelf Research 4 (1/2), 77–103.

Lie, H.-J., 1989. Tidal fronts in the southeastern Hwanghae (Yellow Sea). Continental Shelf Research 9 (6), 527–546.

Lynch, D.R., 1999. Coupled physical/biological models for the coastal ocean. Naval Research Reviews 51 (2), 4–15.

Lynch, D.R., Werner, F.E., Greenberg, D.A., Loder, J.W., 1992. Diagnostic model for Baroclinic and wind-driven circulation in shallow seas. Continental Shelf Research 12, 37–64.

Lynch, D.R., Ip, J.T.C., Naimie, C.E., Werner, F.E., 1995. Convergence studies of tidally-rectified circulation on Georges Bank. In: Lynch, D.R., Davies, A.M. (Eds.), Quantitative Skill Assessment for Coastal Ocean Models, Coastal and Estuarine Series, Vol. 48. American Geophysical Union, Washington, DC, pp. 153–174.

Lynch, D.R., Ip, J.T.C., Naimie, C.E., Werner, F.E., 1996. Comprehensive coastal circulation model with application to the Gulf of Maine. Continental Shelf Research 16 (7), 875–906.

Lynch, D.R., Holboke, M.J., Naimie, C.E., 1997. The Maine coastal current: spring climatological circulation. Continental Shelf Research 17 (6), 605–634.

Lynch, D.R., Naimie, C.E., Hannah, C.G., 1998. Hindcasting the Georges Bank Circulation, Part I: Detiding. Continental Shelf Research 18, 607–639.

Mellor, G.L., Yamada, T., 1982. Development of a turbulence closure model for geophysical fluid problems. Reviews of Geophysics and Space Physics 20, 851–875.

Naimie, C.E., 1996. Georges Bank residual circulation during weak and strong stratification periods - Prognostic numerical model results. Journal of Geophysical Research 101 (C3), 6469–6486.

Naimie, C.E., Loder, J.W., Lynch, D.R., 1994. Seasonal variation of the 3-D residual circulation on Georges Bank. Journal of Geophysical Research 99 (C8), 15,967–15,989.

Naimie, C.E., Lynch, D.R., 1999. Climatological circulation fields for the Yellow Sea. http://www-nml.dartmouth.edu/Data/Yellow–sea.

Nishida, H., 1980. Improved tidal charts for the western part of the north Pacific Ocean. Report of Hydrographic Researches 15, 55–70.

Ogura, S., 1933. The tides in the seas adjacent to Japan. Bulletin of the Hydrographic Department, Imperial Japanese Navy 7, 1–189.

Ogura, S., 1941. Tides. Iwanami Co., Tokyo, Japan (in Japanese).

Riedlinger, S., Preller, R., 1995. Validation test report for the Yellow Sea shallow water analysis and forecast system. Draft NRL Report, Stennis Space Center, MI.

Seung, Y.H., Park, Y.C., 1989. Physical and environmental character of the Yellow Sea. In: Park, C., Kim, D., Lee, S.-H. (Eds.), The Regime of the Yellow Sea-Issues and Policy Options for Cooperation in the Changing Environment. Institute of East and West Studies, Yonsei University, pp. 9–37.

Simpson, J.H., Hunter, J.R., 1974. Fronts in the Irish Sea. Nature 250, 404–406.

Su, J., 1998. Circulation dynamics of the China Seas North of 18 N. In: Robinson, A.R., Brink, K.H. (Eds.),, The Sea, Vol. 11. Wiley, New York, pp. 483–505.

Su, Y.-s., Weng, X.E., 1994. Water masses in China Seas. In: Zhou, D. et al. (Ed.),, Oceanology of China Seas, Vol. 1. Kluwer Academic Publishers, Dordrecht, pp. 3–16.

Sun, Y.L., Chen, S.J., Zhao, K.S., 1990. A three-dimensional baroclinic model of the coastal water. I. Numerical simulation of tidal model and residual currents in the Bohai Sea. Journal of Ocean University of Qingdao 20 (3), 11–24.

Uda, M., 1934. The results of simultaneous oceanographical investigations in the Japan Sea and its adjacent waters in May and June, 1932. Cited by Su (1998). Japanese Imported Fisheries Experimental Station 5, 57–190 (in Japanese).

Xie, L., Hsieh, W.W., Helbig, J.A., 1990. A tidal model of Bohai. Continental Shelf Research 10 (8), 707–721.

Yanagi, T., Inoue, K., 1994. Tide and tidal current in the Yellow/East China Seas. La mer 32, 153–165.

Yanagi, T., Morimoto, A., Ichikawa, K., 1997. Seasonal variation in surface circulation of the East China Sea and the Yellow Sea derived from satellite altimetric data. Continental Shelf Research 17 (6), 655–664.

Yanagi, T., Takahashi, S., 1993. Seasonal variation of circulations in the East China Sea and the Yellow Sea. Journal of Oceanography 49, 503–520.

Yuan, Y., Su, J., 1984. Numerical modelling of the circulation in the East China Sea.. In: Ichiye, T. (Ed.), Ocean Hydrodynamics of the Japan and East China Seas, Oceanography Series, Vol. 39. Elsevier, Amsterdam, pp. 167–186.

Yuan, Y.C., Su, J.L., Xia, S.Y., 1986. A diagnostic model of summer circulation on the northwest shelf of the East China Sea. Progress in Oceanography 17, 163–176.

Yuan, Y.C., Su, J.L., Xia, S.Y., 1987. Three-dimensional diagnostic calculation of circulation over the East China Sea shelf. Acta Oceanologica Sinica 6 (Suppl. I), 36–50.

Zhao, J., Shi, M., 1994. Study on short-range numerical forecasting of ocean current in the East China Sea-II. Three-dimensinal baroclinic diagnostic model and its application in the Bohai Sea. Acta Oceanologica Sinica 13 (2), 173–188.

Zhou, D., Liang, Y.-B., Zeng, C.-K. (Eds.), 1994. Oceanology of China Seas, Vol. 1. Kluwer Academic Publishers, Dordrecht.